

The Aerosol Module in the Community Radiative Transfer Model (v2.2 and v2.3): accounting for aerosol transmittance effects on the radiance observation operator

5 Cheng-Hsuan (Sarah) Lu^{1,2}, Quanhua Liu³, Shih-Wei Wei^{1,2}, Benjamin T. Johnson⁴, Cheng Dang¹,
Patrick G. Stegmann⁴, Dustin Grogan², Guoqing Ge^{5,6}, Ming Hu⁶, and Michael Lueken^{7,8}

¹Joint Center for Satellite Data Assimilation, Boulder, CO, USA

²Atmospheric Sciences Research Center, University at Albany, Albany, NY, USA

10 ³Center for Satellite Applications and Research, NOAA/NESDIS, College Park, MD, USA

⁴Joint Center for Satellite Data Assimilation, College Park, MD, USA

⁵Cooperative Institute for Research in Environmental Sciences, CU Boulder, CO, USA

⁶Global System Laboratory, NOAA, Boulder, CO, USA

⁷I.M. Systems Group, Inc., Rockville, MD, USA

15 ⁸ Environmental Modeling Center, NOAA/NWS/NCEP, College Park, MD, USA

Correspondence to: Cheng-Hsuan Lu (clu@ucar.edu; clu4@albany.edu)

Abstract

The Community Radiative Transfer Model (CRTM), a sensor-based radiative transfer model, has been used within the
20 Gridpoint Statistical Interpolation (GSI) system for directly assimilating radiances from infrared and microwave sensors. We
conducted numerical experiments to illustrate how including aerosol radiative effects in CRTM calculations changes the GSI
analysis. Compared to the default aerosol-blind calculations, the aerosol influences reduced simulated brightness temperature
(BT) in thermal window channels, particularly over dust-dominant regions. A case study is presented, which illustrates how
failing to correct for aerosol transmittance effects leads to errors in meteorological analyses that assimilate radiances from
25 satellite IR sensors. In particular, the case study shows that assimilating aerosol-affected BTs significantly affects analyzed
temperatures in the lower atmosphere across several regions of the globe. Consequently, a fully-cycled aerosol-aware
experiment improves 1-5 day forecasts of wind, temperature, and geopotential height in the tropical troposphere and Northern
Hemisphere stratosphere. Whilst both GSI and CRTM are well documented with online user guides, tutorials and code
repositories, this article is intended to provide a joined-up documentation for aerosol absorption and scattering calculations in
30 the CRTM and GSI. It also provides guidance for prospective users of the CRTM aerosol option and GSI aerosol-aware
radiance assimilation. Scientific aspects of aerosol-affected BT in atmospheric data assimilation are briefly discussed.

1 Introduction

35 An accurate and computationally efficient radiative transfer model is essential in radiance assimilation for supporting weather prediction, physical retrievals for satellite environmental data records, and inter-comparison between different remote sensing instruments. The Community Radiative Transfer Model (CRTM) is a radiative transfer model used extensively within satellite and remote sensing systems (Weng, 2007; Han et al., 2007). It was primarily designed for computing satellite radiances and has been widely used within the Gridpoint Statistical Interpolation (GSI, Wu et al., 2002; Kleist et al., 2009) system for directly assimilating radiances from infrared (IR) and microwave (MW) sensors. Specifically, clear-sky radiance calculations are carried out within the CRTM given the atmospheric scattering and absorption profile, surface emissivity and reflectivity, and source functions. For cloudy radiance simulations (Stegmann et al., 2018), vertical profiles of hydrometeor variables (e.g., cloud liquid water path and ice water path) are also required. Note that the CRTM was not designed to enact composition-radiation interaction effects within spectral longwave and shortwave radiative transfer calculations in general circulation models. Instead, the CRTM was developed to support monochromatic satellite radiance assimilation from longwave and microwave sensors, and for satellite retrieval algorithm development.

45 Past studies have demonstrated that aerosols significantly impact the simulation of brightness temperature (BT) in the IR channels. BT is “a descriptive measure of radiation in terms of the temperature of a hypothetical blackbody emitting an identical amount of radiation at the same wavelength” (American Meteorological Society, 2012). A reduction in retrieved BT of 2-4 K in the atmospheric window region due to a strong dust outbreak was reported during the Saharan Dust Experiment (SHADE) campaign (Highwood et al., 2003). Pierangelo et al. (2004) and Peyridieu et al. (2009) showed that the dust cooling effects may reach 3 K in tropical atmospheric conditions depending on the dust burden. Diaz et al. (2001) found that there is a significant increase in the errors of sea surface temperature (SST) retrievals in the presence of enhanced aerosol loading in the atmosphere. The dust effects on satellite derived SST are constrained by accounting for dust absorption (Weaver et al., 2003), applying a dust correction scheme (Nalli and Stowe, 2002; Merchant et al., 2006), or removing dust-contaminated observations (Divakarla et al., 2012).

The impact of aerosol-affected BTs on the meteorological analysis fields has also been investigated. Wei et al. (2021a) used the Global Data Assimilation System (GDAS, Kleist et al., 2009) to assess the aerosol impact on the meteorological analysis. To do this, two GDAS experiments were conducted: a control cycled experiment, where aerosol transmittance effects are not considered, and an offline non-cycled experiment, where aerosol transmittance effects are considered in the BT calculations. The offline experiment uses identical observations and first guesses as the control experiment and thus the response of atmospheric analysis to aerosol-aware radiance calculations can be clearly demonstrated. The experimental setup in Wei et al. (2021a) followed the methodology presented in Kim et al. (2018), which is based on the Goddard Earth Observing System (GEOS)-atmospheric data assimilation system (ADAS). Note that GEOS-ADAS and GDAS both used GSI and CRTM,

65 although the version and configuration differed. The studies by Kim et al. (2018) and Wei et al. (2021a) reported that: (i) a
considerable cooling effect on simulated BT when aerosols are considered; (ii) including aerosol transmittance effects in the
BT calculation improves the fit to observations over the dust-laden regions, and (iii) the offline aerosol-aware experiment
produces warmer analyzed SST (0.3 - 0.5 K) over the Atlantic Ocean. Wei et al. (2021a) also reported a warmer analysed
lower atmosphere (0.15 K) over Africa and the central Atlantic Ocean in the offline aerosol-aware experiment.

70

The experiments conducted in Kim et al. (2018) and Wei et al. (2021a) were based on the application of the CRTM aerosol
absorption and scattering routines. While aerosol absorption and scattering options are available from CRTM version 2.2
onwards; to our knowledge, the documentation of the CRTM aerosol module (Liu and Lu, 2016) has yet to be updated. Here
we presented a joined-up documentation for aerosol absorption and scattering calculations in the CRTM and GSI. In addition,
75 we provide guidance for prospective users of running aerosol-affected GSI analysis. Scientific aspects of aerosol-affected BT
in atmospheric data assimilation are also briefly discussed.

2 GSI and CRTM

Below, we provide a brief introduction to the GSI in section 2.1 and a description of the CRTM aerosol option in section 2.2.
In section 2.3, a description of running aerosol-aware GSI analysis is given.

80 2.1 GSI

The multi-partner-developed GSI is an incremental three-dimensional variational (3D-Var) data assimilation system (Wu et
al., 2002; Kleist et al. 2009). GSI, alone or combined with an ensemble system, has been used widely by modelling centers
and the research community for a range of research and applications. For instance, it is used operationally by the National
Oceanic and Atmospheric Administration (NOAA)/National Centers for Environmental Prediction (NCEP) for medium-range
85 weather forecast. It is also used by the National Aeronautics and Space Administration (NASA)/Global Modeling and
Assimilation Office (GMAO) for recent production of the Modern-Era Retrospective Analysis for Research and Applications,
version 2 (MERRA-2; Gelaro et al., 2017). The community version of the GSI system has been supported and maintained by
the Developmental Testbed Center (DTC; <http://www.dtcenter.org>). Note that DTC is scheduled to cease all activities
supporting the GSI user community by the end of December 2021. However, community GSI-related assets (website, forum,
90 and repository) built by DTC will remain available to and usable by the community.

GSI can assimilate a wide range of observations, including conventional observations (such as radiosonde observations), radar
data, satellite retrievals (for example global positioning system (GPS) radio occultation sounding data), satellite radiance data,
etc. For IR satellite instruments, GSI has the capability to assimilate radiances from Advanced Infrared Sounder (AIRS) on
95 AQUA, Infrared Atmospheric Sounding Interferometer (IASI) on METOP-A and METOP-B, Cross-track Infrared Sounder

(CrIS) on S-NPP, High resolution Infrared Radiation Sounder (HIRS) on METOP-A, METOP-B, and NOAA-19, Advanced Very High Resolution Radiometer (AVHRR) on NOAA-18 and METOP-A, Spinning Enhanced Visible and Infrared Imager (SEVIRI) on M08 and M10, and Geostationary Operational Environmental Satellite (GOES) Sounders (s ndrD1, s ndrD2, s ndrD3, and s ndrD4) on GOES-15. A comprehensive list of all observations assimilated and monitored by GDAS can be found at the webpage for “Observational Data Processing at NCEP” (<https://www.emc.ncep.noaa.gov/emc/pages/infrastructure/obs-data-processing.php>).

Despite the broad applications of GSI, the publicly released version handles only clear-sky radiances for IR sensors. Without correcting for aerosol transmittance effects, systematic biases may be introduced into the meteorological analysis fields when observations affected by aerosols are assimilated. The aerosol-aware option (discussed in section 2.2) reduces such errors by enabling aerosols to influence GSI’s radiance observation operator, CRTM, which calculates the BT and Jacobians (radiance 1st derivative). This option, however, may fluctuate the amount of observations assimilated in GSI because the quality control (QC) algorithm screens out observations based on measured BTs and aerosol-free simulated BTs. Thus, an improved QC algorithm is needed to fully exploit radiance measurements under all sky conditions. The technical issues regarding the QC procedure have been discussed in Kim et al. (2018) and Wei et al. (2021a).

2.2 CRTM aerosol module

The CRTM, a one-dimensional radiative transfer model (Liu and Weng, 2006), is developed at the U.S. Joint Center for Satellite Data Assimilation (JCSDA) with algorithm and software input from JCSDA collaborating research institutions. The CRTM is composed of four modules, which include gaseous transmittance, surface emission and reflection, cloud and aerosol absorption and scattering, and a solver for radiative transfer (Han et al., 2006). Given an atmospheric profile of temperature, cloud and surface properties, and gaseous constituents and aerosol concentrations, the CRTM is called within the GSI to calculate BTs for satellite sensors from IR sounders to MW imagers. Here, we describe the aerosol scattering and absorption scheme in CRTM version 2. We refer the readers to Han et al. (2006) for the full details regarding CRTM version 1.

Absorption by atmospheric trace gases, such as water vapor and carbon dioxide, is parameterized using the Optical Depth in Absorber Space (ODAS) and the Optical Depth in Pressure Space (ODPS) algorithms (Chen et al., 2012), which are based on rigorous line-by-line calculations from the Line-By-Line Radiative Transfer Model (LBLRTM, Clough et al., 1992). For enacting aerosol attenuation effects, the CRTM uses pre-computed lookup tables, which calculate aerosol optical properties, specifically the extinction coefficient, single-scattering albedo, asymmetry factor, and phase function coefficients. The CRTM version 2.2 and 2.3 contain the optical look-up table based on the aerosol types of the mass-based Goddard Chemistry Aerosol Radiation and Transport (GOCART, Chin et al., 2002; Colarco et al, 2010) module, for their radiative effects from the ultraviolet to the infra-red. Operationally, given aerosol types, radius, concentration and ambient relative humidity, CRTM generates aerosol optical profiles that the radiative transfer solver requires for multi-scattering simulations and radiance

calculations. The effect of aerosols on MW sensors is not considered yet because the impact of aerosols on MW radiance is usually very small, given aerosols size is generally much smaller than MW wavelengths (Petty, 2006). There are ongoing and planned CRTM development efforts to incorporate more aerosol optical tables (such as the Community Multiscale Air Quality model, CMAQ). With the expansion of the aerosol schemes, a new releasing and versioning system for optical tables is essential and currently under discussion. This article, however, discusses mainly the GOCART model, which is the default aerosol scheme in the CRTM version 2.

The GOCART model (Chin et al., 2002; 2014), a bulk aerosol scheme, simulates major tropospheric aerosol components, including dust, sea salt, black carbon (BC), organic carbon (OC) and sulfate. It is one of the most widely used aerosol modules in the Weather Research and Forecasting model coupled with Chemistry (WRF-Chem; see Ukhov et al. (2021) and references therein). It is used in the GEOS framework at GMAO for near-real-time aerosol forecasts (Colarco et al., 2010) as well as in MERRA reanalysis (Buchard et al., 2015) and MERRA-2 reanalysis (Randles et al., 2017). It is also implemented in the Global Forecast System (GFS) framework at NCEP (Lu et al., 2016; Wang et al., 2018; Zhang et al., 2021) for near-real-time global aerosol forecasts.

When GOCART was selected as the aerosol module within WRF-Chem, it was configured with fourteen GOCART aerosol species (Liu et al., 2011): sulfate; hydrophobic and hydrophilic OC and BC; sea salt in four particle size bins (with radii of 0.1-0.5, 0.5-1.5, 1.5-5, and 5-10 μm) and dust particles in five particle size bins (with radii of 0.1-1.0, 1.0-1.8, 1.8-3, 3-6, and 6-10 μm). A default CRTM lookup-table has been used for pre-calculated aerosol optical property parameters for the fourteen GOCART aerosol species (Liu et al., 2007; Liu and Lu, 2016). We assume that the particles are spherical and externally mixed. We also assume lognormal size distributions for sulfate and carbonaceous aerosols as well as for each sea salt and dust bin. The lognormal size distribution for N particles can be expressed as follows (d'Almeida et al., 1991),

$$n(\ln r) = \frac{N}{\sqrt{2\pi \ln(\sigma_g)}} \exp\left[-\frac{1}{2} \left(\frac{\ln r - \ln r_g}{\ln(\sigma_g)}\right)^2\right], \quad (1)$$

where r is a radius, r_g the geometric median radius, and σ_g the geometric mean standard deviation. The k^{th} moment of the distribution can be expressed as follows (Binkowski and Roselle, 2003),

$$M_k = \int_{-\infty}^{\infty} r^k n(\ln r) d\ln(r) = r_g^k \exp\left[\frac{k^2}{2} \ln^2(\sigma_g)\right] \quad (2)$$

where M_0 is the number N of aerosol particles, and M_2 and M_3 are proportional to the total particulate surface area and volume, respectively. Thus, the effective radius (r_{eff}) can be defined as

$$r_{\text{eff}} = \frac{M_3}{M_2} = r_g \exp\left[\frac{5}{2} \ln^2(\sigma_g)\right] \quad (3)$$

160 Table 1 lists the GOCART size parameters (particle density, effective radius, and geometric standard deviation) and refractive indices at 550 nm used in CRTM version 2. The optical properties of each aerosol species are computed based on Mie scattering theory. Hydrophilic aerosol particle size increases as relative humidity (RH) of the ambient atmosphere increases. Therefore, the water content in aerosol needs to be considered when calculating the refractive index. The effective radius growth factor for hygroscopic aerosols may be theoretically calculated or obtained from a pre-calculated look-up table (d’Almeida et al., 1991). In this study, the hygroscopic growth factor used for the GOCART model (Chin et al., 2002) is adopted and given in 165 Table 2. Once the growth factor a_g is evaluated, the refractive index n_r for the hygroscopic aerosol can be calculated using a volume mixing method as:

$$n_r = n_w + (n_o - n_w) \times a_g^3 \quad (4)$$

170 where n_o and n_w are the refractive indices for dry aerosols and water, respectively. We adopt the refractive index n_o from the Optical Properties of Aerosols and Clouds (OPAC) dataset (Hess et al. 1998), while the water refractive index is given by (Hale and Querry, 1973).

Table 1. Goddard Chemistry Aerosol Radiation and Transport (GOCART) size distribution parameters and refractive indices at 550 nm for dry aerosols.

Aerosol type	Density [g cm ⁻³]	Effective radius r_{eff} [μm]	Standard deviation σ [μm]	Refractive index real part $n(\lambda)$	Refractive index imaginary part $k(\lambda)$
Sulfate	1.7	0.242	2.03	1.43	1.00×10^{-8}
OC1 (hydrophobic)	1.8	0.087	2.20	1.53	6.00×10^{-3}
OC2 (hydrophilic)	1.8	0.087	2.20	1.53	6.00×10^{-3}
BC1 (hydrophobic)	1.0	0.036	2.0	1.75	4.40×10^{-1}
BC2 (hydrophilic)	1.0	0.036	2.0	1.75	4.40×10^{-1}
SeaSalt1 (size range)	2.2	0.3	2.03	1.50	1.00×10^{-8}
SeaSalt2	2.2	1.0	2.03	1.50	1.00×10^{-8}
SeaSalt3	2.2	3.25	2.03	1.50	1.00×10^{-8}
SeaSalt4	2.2	7.5	2.03	1.50	1.00×10^{-8}
Dust1 (size range)	2.6	0.65	2.0	1.53	5.50×10^{-3}
Dust2	2.6	1.4	2.0	1.53	5.50×10^{-3}
Dust3	2.6	2.4	2.0	1.53	5.50×10^{-3}
Dust4	2.6	4.5	2.0	1.53	5.50×10^{-3}
Dust5	2.6	8.0	2.0	1.53	5.50×10^{-3}

175 **Table 2.** Hygroscopic aerosol growth factor a_g as a function of the ambient relative humidity (RH).

RH(%)	0	50	70	80	90	95	99

Sulfate	1.0	1.4	1.5	1.6	1.8	1.9	2.2
Organic Carbon	1.0	1.2	1.4	1.5	1.6	1.8	2.2
Black Carbon	1.0	1.0	1.0	1.2	1.4	1.5	1.9
Sea Salt	1.0	1.6	1.8	2.0	2.4	2.9	4.8

The GOCART model used by GMAO and NCEP for aerosol forecast and reanalysis has evolved to use 5 sea salt size bins (with radii of 0.03-0.1, 0.1-0.5, 0.5-1.5, 1.5-5, and 5-10 μm). The first sub-micron sea salt bin was added to facilitate optical properties and aerosol-cloud interaction studies (Colarco et al., 2010), but was excluded from the previous GOCART versions as well as the WRF-Chem GOCART model. While GMAO's GEOS and NCEP's GFS contain fifteen GOCART aerosol species, the CRTM aerosol module has also not yet been modified to include the new added sub-micron sea salt bin (see Table 1). To overcome this discrepancy, the latest GSI/CRTM release (i.e., GSI 3.7 and CRTM 2.3) combines the mixing ratios from the two sub-micron sea salt bins in order to use the aerosol optical property parameters from the original GOCART model. This limitation is acknowledged in this article and will be addressed in a future CRTM release (see section 4).

While the CRTM is primarily designed for computing satellite radiances, an additional module was added to CRTM by Liu and Lu (2016) to compute aerosol optical depth (AOD). This CRTM-AOD module enables the GSI system to assimilate AOD observations (Liu et al., 2011; Schwartz et al., 2012; Pagowski et al., 2014). This article, however, is focused on the observation operator for radiance, and we refer the reader to Pagowski et al. (2014) for the description of the AOD observation operator and GSI AOD data assimilation.

2.3 Running aerosol-aware GSI analysis

The operational version of GSI maintained by NOAA/NCEP Environmental Modeling Center (EMC) is utilized in the present study. Its source code and associated static files are distributed through the GitHub repository (<https://github.com/NOAA-EMC/GSI>). An open-access archive of source code and data is described in Code and Data Availability. To run the GSI analysis, the reader can refer to the user guide for GSI v3.7 (the latest released version as of April 2021), which is available at https://dtcenter.ucar.edu/com-GSI/users/docs/users_guide/html_v3.7/index.html. In addition, an online tutorial is available at https://dtcenter.ucar.edu/com-GSI/users/tutorial/online_tutorial/index_v3.7.php. For CRTM, the user guide and tutorials can be found at <https://www.jcsda.org/jcsda-project-community-radiative-transfer-model>. Thus, only a brief description of aerosol-affected BT calculations is given.

A regression test "global_C96_fv3aerorad" has been introduced into NOAA/EMC GSI code repository (pull request #32) to assure the functionality of aerosol-aware BT derivations in GSI/CRTM works as expected. This regression test uses a sample background file taken from the aerosol member of the Global Ensemble Forecast System (GEFS-Aerosol; Zhang et al., 2021). All fifteen GOCART aerosol species are passed along to the CRTM. In addition to the background file, a user needs to modify

205 the configuration files, anavinfo and satinfo, in the “fix” directory. The anavinfo file is the information file to set control and analysis variables. The satinfo file is the information file to specify satellite channels to be assimilated and associated parameters. For an aerosol-aware experiment where aerosol absorption and scattering are included in BT calculations, aerosol species are specified in the “chem_guess” section of anavinfo and sensors and channels are set to 1 in the “iaerosol” column of satinfo. The reader can refer to the fv3aerorad_satinfo.txt and anavinfo_fv3aerorad for the aerosol-aware configuration. The
210 corresponding namelist (gsiparm.anl) can be found at the “global_C96_fv3aerorad” section (line 2931–3046) in regression_namelist.sh under the “regression” directory. It should be noted that the namelist variable, “lread_ext_aerosol”, determines how GSI ingests the aerosol information from background files or external files.

3. Numerical Results

3.1 Aerosol impacts on BT calculations

215 To illustrate how an aerosol transmittance correction is required within satellite radiances assimilated into meteorological data assimilation systems, we present a detailed analysis of a single-cycle GSI experiment (the AER experiment) using GOCART fields from MERRA-2 on 12Z June 22, 2020. This time is chosen because it captures a strong Saharan dust event that covers the trans-Atlantic region. A baseline GSI experiment (the CTL experiment) with the anavinfo and satinfo resource files reverted back to the default aerosol-blind configuration was also conducted. Both experiments used the same first-guess fields and
220 assimilated identical conventional and satellite observations within a ± 3 -hour assimilation window. In AER, the aerosol transmittance effects were only considered in the CRTM simulation for IR sensors.

Figure 1 shows the global aerosol column mass density distribution from MERRA-2 during 12Z June 22, 2020. The panels a, b, c, and d depict dust, sea salt, carbonaceous and sulfate, respectively. Dust plumes spread over northern Africa, the tropical
225 Atlantic Ocean, the Middle East, and northwestern China. Wind-driven sea salt aerosols are seen over tropical and southern hemisphere oceans. Carbonaceous and sulfate aerosols mainly appear in areas with extensive biomass burning and fuel combustion activities (note one order smaller than dust and sea salt). The overall aerosol loading is dominated by mineral dust. Wu et al. (2020) evaluated the dust spatiotemporal variations of MERRA-2 against satellite observations and global model simulations. They found that MERRA-2 agrees well with satellite observations due to the assimilation of satellite AOD. But
230 in North America and the Arctic, the dust burden in MERRA-2 is much larger than those in other models despite having similar dust emissions fluxes. The high dust burden over these regions is due to higher mass fraction of fine dust and enhanced dust transport. Furthermore, Bullard et al. (2016) reported that large gaps exist in our understanding of basic characteristics of high-latitude dust sources. This highlights the importance of representing aerosol emissions, transport, removal, and size distribution in global models in correctly simulating aerosol spatiotemporal distributions.

235

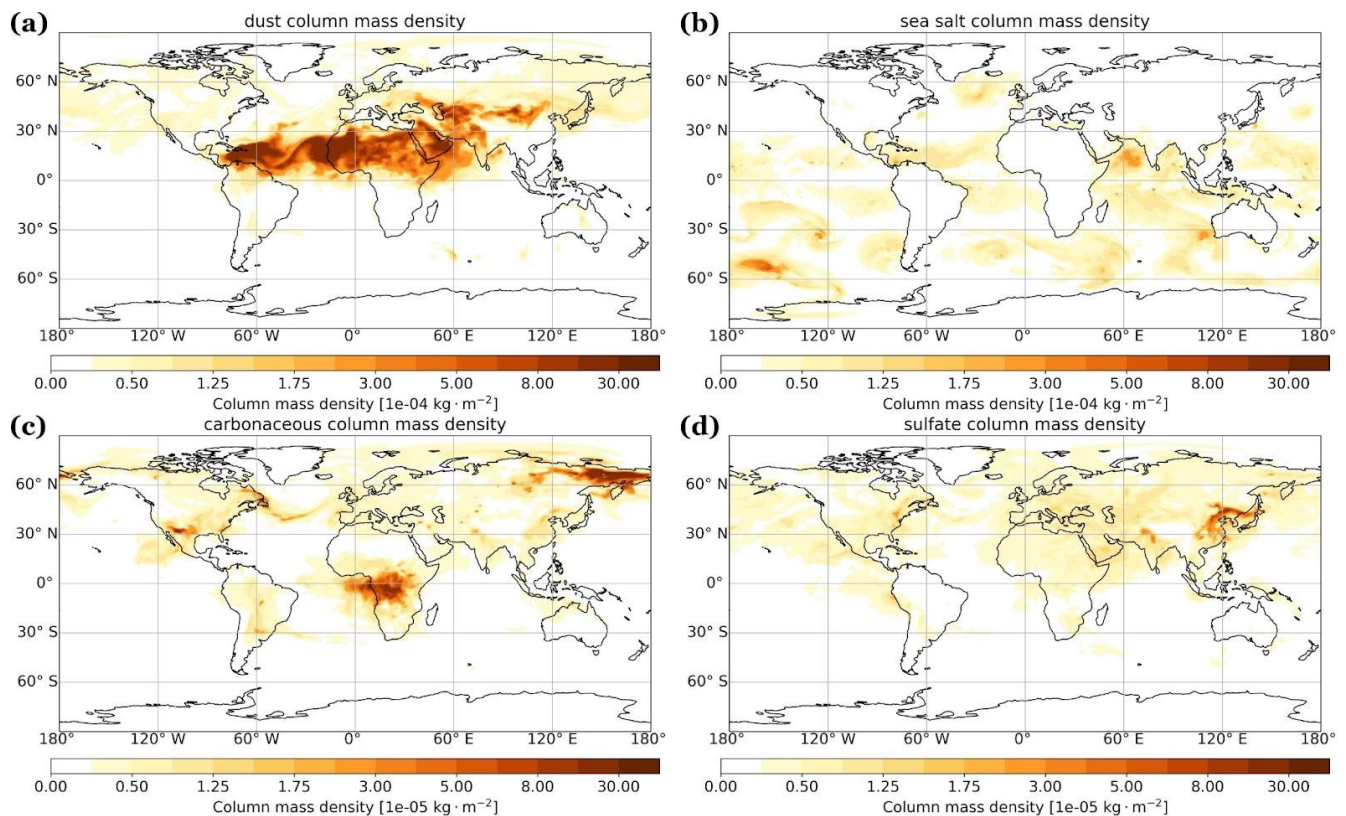


Figure 1. Aerosol column mass density (kg m^{-2}) from MERRA-2 on 12Z June 22, 2020: (a) dust, (b) sea salt, (c) carbonaceous, and (d) sulfate.

240 Figure 2a shows the first-guess BT differences of IASI onboard METOP-A between the two experiments (AER – CTL) in the IR atmospheric window channels over dust, sea salt, carbonaceous and sulfate dominant regions. The stratification criterion for each type is where the fraction of column mass density of dominant species, from MERRA-2, is larger than 0.65 (shown in Fig. 2b). Figure 2a shows that dust aerosols generate the stronger cooling effects, about 0.7 K at the thermal IR window region ($\sim 10 \mu\text{m}$), than other species. The importance of correcting for aerosol transmittance effects within BT algorithms has been reported in previous studies (Sokolik, 2002; Weaver et al., 2003; Pierangelo et al., 2004; Matricardi, 2005; Merchant et al., 2006; Kim et al., 2018; Wei et al., 2021a). Table 3 describes the range and the average of total aerosol column mass density over the regions with different dominant aerosol species. It shows that the total loading of aerosols is similar over the dust and carbonaceous aerosols dominated regions. This indicates that the stronger cooling effects by dust aerosol on BT in the IR window region is not due to stronger loading. Note that in the northern hemisphere, the high-latitude region is characterized as dust-dominant except for the Russian Far East in MERRA-2 (Figure 2b). While anomalous or erroneous modeled aerosol loading may bias the results, the finding that dust has the largest impact on the BTs simulations, reported in this study and

245

250

previous studies, remains unchanged. Therefore, we focus our remaining analysis on dust over Tropical Africa and the Mid-Atlantic.

255

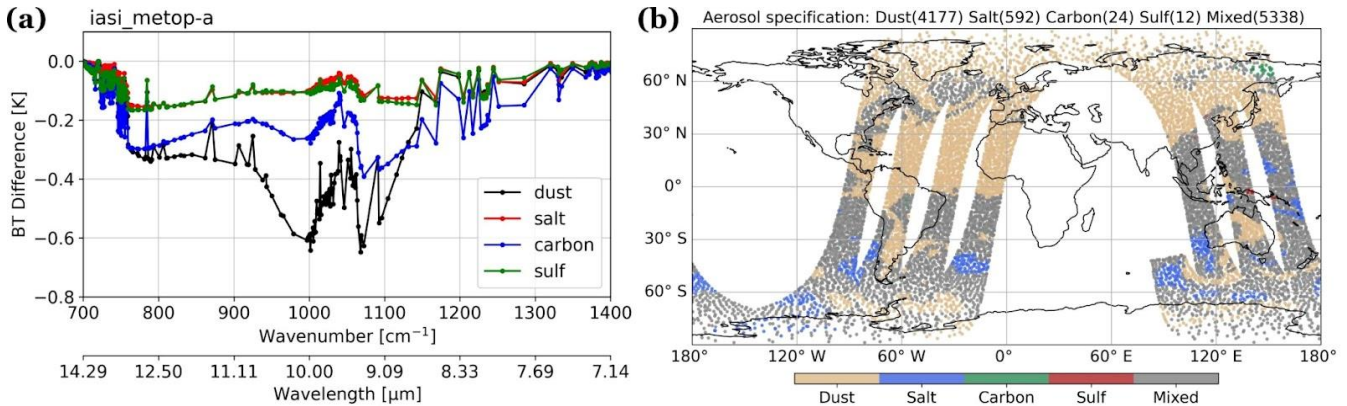


Figure 2. (a) The differences (AER-CTL) of first-guess brightness temperatures in the IR window region of IASI onboard METOP-A. (b) The corresponding regions dominated by different aerosol species from the 12Z June 22, 2020. The data counts for each species are labelled in panel (b).

260

Table 3. The range of aerosol column mass density (kg/m^2) from MERRA-2 at the regions dominated by different aerosol species (fraction over 0.65) of IASI onboard METOP-A at the cycle of 12Z June 22, 2020.

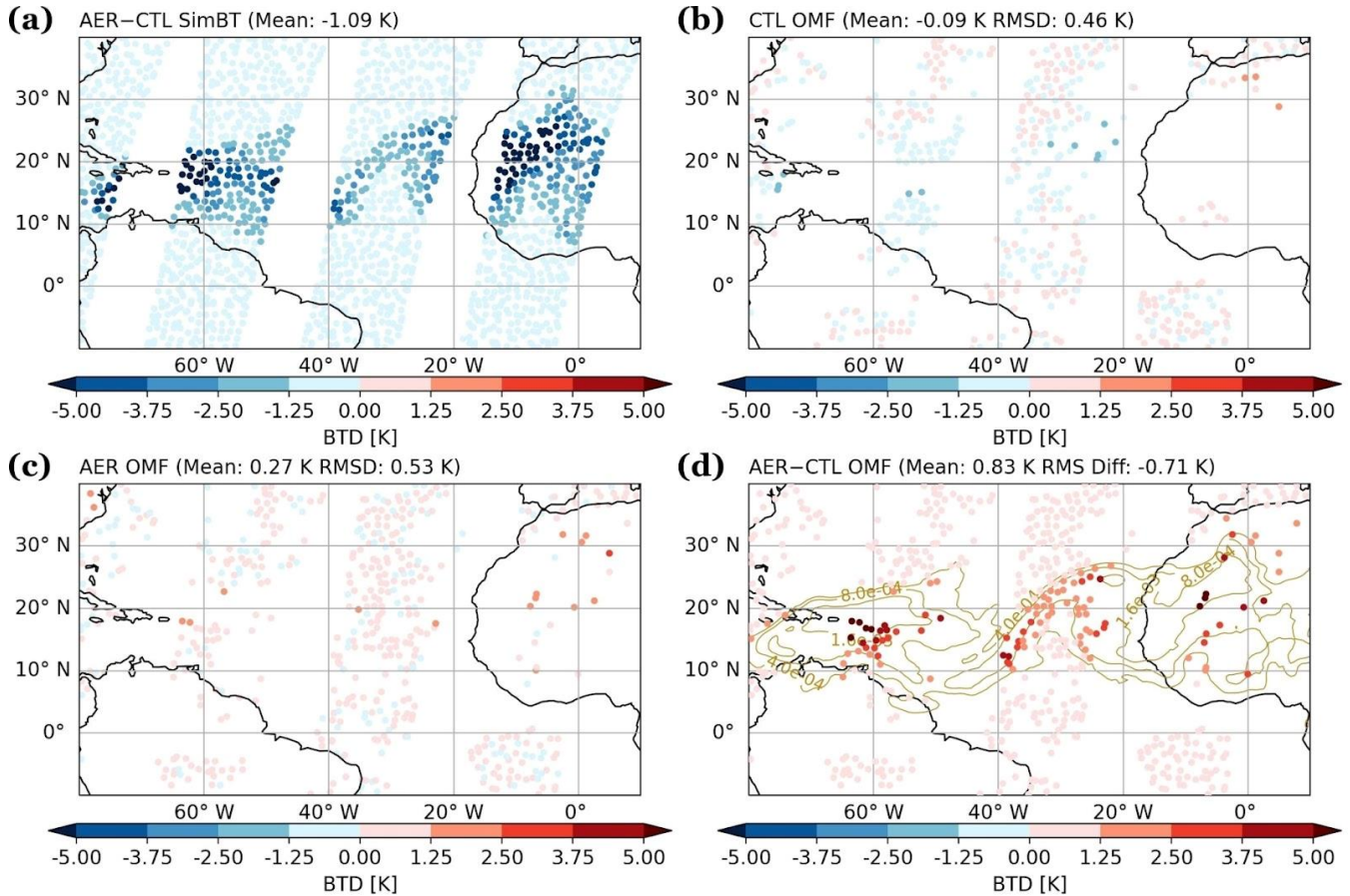
Dominant aerosol species	Column mass density (kg/m^2)				
	Minimum	Maximum	Mean	Median	SD
Dust	2.69e-06	2.88e-03	1.76e-04	4.20e-05	3.59e-04
Sea salt	4.91e-06	4.01e-05	1.68e-05	1.59e-05	6.15e-06
BC+OC	1.04e-05	6.07e-04	1.76e-04	1.52e-04	1.20e-04
Sulfate	6.45e-06	9.53e-05	2.15e-05	1.28e-05	2.46e-05

265

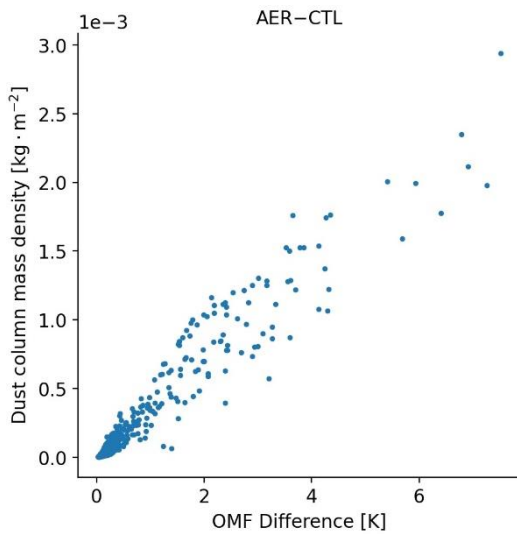
Figure 3 displays the AER - CTL difference in the simulated BTs and their respective first-guess departures (observed minus first guess, OMF) calculated at the $10.39 \mu\text{m}$ channel from IASI onboard METOP-A. The Figure focuses on North Africa and the trans-Atlantic region, where a large dust plume spans the region. Significant aerosol cooling ($\sim 4 \text{ K}$) in BT was found in the aerosol-aware experiment (Fig. 3a) due to the large plume. Comparing the first guess departures from CTL and AER experiments (Fig. 3b and 3c) shows that OMFs for AER are warmer than CTL (cf. 0.27 K vs. -0.09 K). Note that some observations assimilated in CTL were rejected in AER (near 55° W and 15° N) and vice versa (near 65° W and 15° N , and

270 over Africa). This feature suggests that the quality control has been influenced by including aerosol transmittance effects in CRTM. Over the trans-Atlantic region, the aerosol-aware experiment assimilated several observations with larger first-guess departures located in the strong dust plume (Fig. 3d). Figure 4 presents the scatter plot of dust column mass density versus OMF differences (AER - CTL) for these data points assimilated in AER on 12Z June 22, 2020. The data points with large OMF differences are corresponding to the areas with higher dust loading. Nevertheless, when considering aerosol information, the root-mean-square first-guess departures decreased 0.08 K globally and 0.42 K over the trans-Atlantic region at this channel (not shown here). This implies that simulated BTs in the aerosol aware run are in better agreement with the observations.

275



280 **Figure 3.** (a) Simulated BT differences (AER - CTL), (b) bias-corrected OMF from the CTL experiment, (c) bias-corrected OMF from the AER experiment, and (d) OMF differences (AER - CTL) for 10.39 μm channel of IASI onboard METOP-A. All the data are from the analysis cycle on 12Z June 22, 2020. Contours of total column mass density from MERRA-2 are plotted in panel (d).



285 **Figure 4.** The scatter plot of dust column mass density from MERRA-2 against the first-guess departure differences (AER – CTL) assimilated in AER experiment (without bias correction) on 12Z June 22, 2020.

Figure 5 shows (a) the global differences in analyzed temperature at 900 hPa between the two experiments and (b) the total aerosol column mass density incorporated in the GSI/CRTM system. When aerosol transmittance effects are considered in the BT calculations, the air temperatures are not only adjusted over aerosol-laden regions but also across the globe. The impact is shown outside aerosol-active regions, which could be attributed to the change from the spatial correlation in the GSI background error covariance. Over the trans-Atlantic region where the dust loading is high (shown in Figure 1a), the AER experiment produces 0.5 K to 1 K of warming relative to CTL. As dust travels off the west coast of Africa into the Atlantic, the particles are lifted and carried by the Saharan Air Layer (SAL), around 800 – 600 hPa (Diaz et al., 1976; Karyampudi et al., 1999). In the case of 12Z June 22, 2020, MERRA-2 captured the dust transport within SAL, and air mass is increasingly composed of fine dust particles due to the gravitational settling of coarser particles (not shown here). Wei et al. (2021b) conducted a series of CRTM v2.3 experiments using idealized dust profiles and reported that mass loading and the altitude of the dust layer are the primary and secondary factors affecting the BT simulations, respectively; changes in the fine versus coarse particle partition show little influence on the BT simulations. Based on these results we speculate that elevated dust plume retains unneglected influences on BT calculations (Figure 3a). Experiments with robust estimated aerosol distributions over extended time period are needed to quantify the sensitivity of GSI analysis to aerosol-aware CRTM calculations. This manuscript, however, is intended to provide a joined-up documentation for the CRTM aerosol option and thus unravelling these questions is beyond the scope of this study.

305

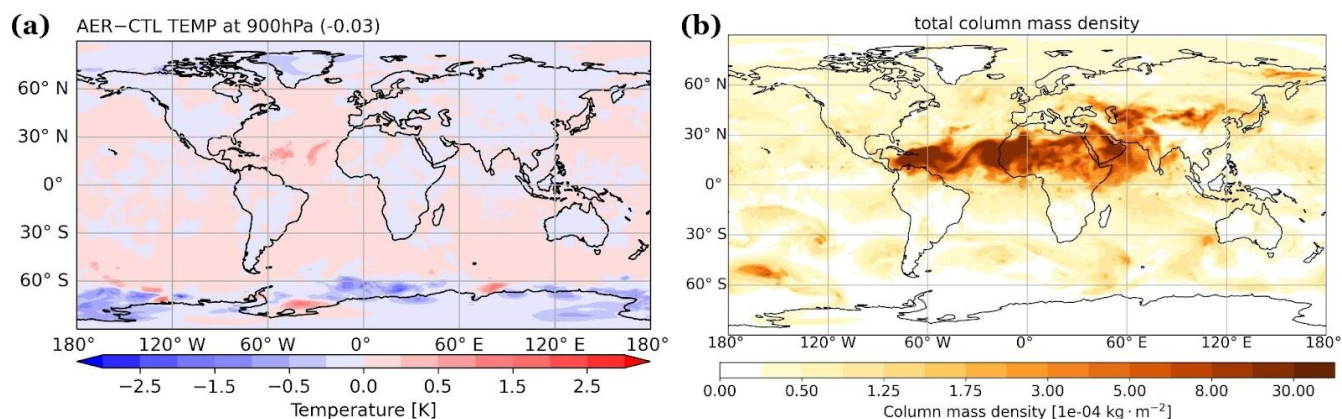


Figure 5. (a) The differences (AER - CTL) of analyzed temperature (K) at 900 hPa and (b) the corresponding aerosol column mass density (kg m^{-2}) from MERRA-2 on 12Z June 22, 2020.

3.2 Aerosol impacts on the analysis

310 The experiments reported in this section were produced with the NCEP GFS version 14 and the corresponding GDAS. Our experiments used a coarser resolution, T670 (~ 30 km) for the model and T254 (~ 80 km) for the analysis, different from the NCEP operational GFSv14 configuration at T1534 (~ 13 km) and T574 (~ 27 km). The experiments covered the August 2017 period, initialized from NCEP's archived GDAS analysis on July 25 00Z. The analysis cycles every 6 hours (at 00z, 06z, 12z, and 18z), with a ± 3 -hour assimilation window and continuous data utilization. The control experiment (CTL_cyc) was an aerosol-blind fully cycled experiment where aerosol effects on radiances are not considered (as is by default). The aerosol experiment (AER_cyc) was an aerosol-aware fully cycled experiment where aerosol-affected satellite radiances are taken into account. Here, we used CRTM version 2.2.4. Time-varying 3-dimensional GOCART aerosols were taken from NCEP's archived NEMS GFS Aerosol Component (NGAC) v2 (Wang et al., 2018).

320 Figure 6 displays the statistics of analysis departures (observation minus analysis, OMA) from CTL_cyc and AER_cyc to evaluate the performance of temperature analysis at the lower atmosphere over the tropical region ($20^\circ \text{S} - 20^\circ \text{N}$). The positive value of mean OMAs indicates that both experiments have cold biases in the tropical region. It shows neutral impact on root-mean-square (RMS) and slightly positive impact on the cold biases. The latter implies that the departure of temperature analysis becomes larger when considering aerosol transmittance effects during the data assimilation (i.e., AER_cyc).

325

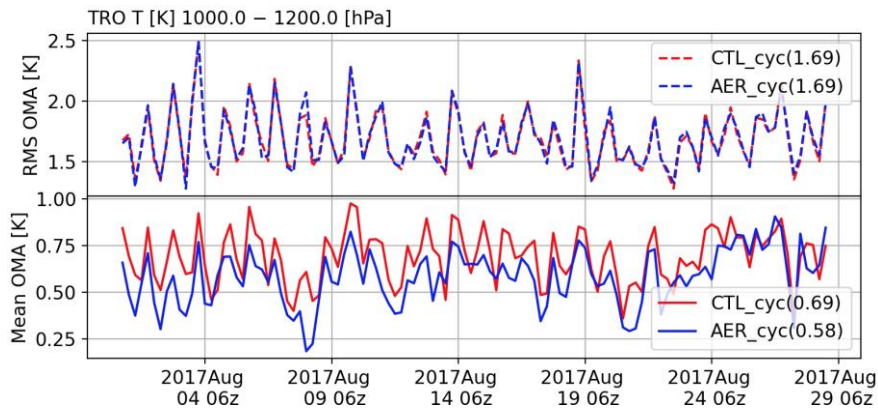


Figure 6. The comparison of the RMS and mean analysis departures (observation minus analysis, OMA) against in-situ measurements (e.g., radiosonde) of temperature with pressure over 1,000 hPa at the tropical region (20° S – 20° N) during 00Z August 1 – 18Z August 28, 2017.

330

Medium-range forecasts of AER_cyc are examined against CTL_cyc using the verification package from NOAA/NCEP EMC (https://www.emc.ncep.noaa.gov/gmb/STATS_vsdb). Figure 7 displays the scorecard of anomaly correlation and root-mean-square error (RMSE) for the day-1, -3, and -5 forecasts over August 1 – 28, 2017. Anomaly correlation coefficients show neutral to positive impact on day-1 forecasts of wind and temperature fields when aerosol cooling effects in BTs are considered.

335

The RMSE scorecards show the forecast improvements in the wind, temperature and height fields throughout the troposphere over the Tropics (20° S – 20° N) and at upper level over the Northern Hemisphere (20° N – 80° N). For the Southern hemisphere (20° S – 80° S), however, there is neutral impact or degradation in the forecasts, which is likely due to cloud contamination and mixture of sea salt and aged smoke/sulfate aerosols. Compared to both hemispheres, the tropical forecasts show the most improved statistics in the aerosol-aware analysis, which may be attributed to larger aerosol loading in this region. While the RMSE scorecard focuses on background (i.e., time-averaged) fields, it should be noted that evaluation of the aerosol impacts on the analysis and forecasts of African easterly wave that developed Hurricane Harvey and Gert in 2017 is presented in Grogan et al. (2021).

340

		Globe			N. Hemisphere			S. Hemisphere			Tropics				
		Day 1	Day 3	Day 5	Day 1	Day 3	Day 5	Day 1	Day 3	Day 5	Day 1	Day 3	Day 5		
Anomaly Correlation	Heights	250hPa													
		500hPa													
		700hPa													
		1000hPa													
	Vector Wind	250hPa	▲												
		500hPa	▲												
		850hPa	▲												
	Temp	250hPa	▲						▲						
		500hPa		▼						▼					
		850hPa	▲			▲									
RMSE	Heights	10hPa	▲	▲	▲		▲	▲				▲	▲	▲	
		20hPa	▲	▲	▲	▲	▲	▲				▲	▲	▲	
		50hPa	▲	▲	▲	▲	▲	▲	▲				▲	▲	▲
		100hPa	▲	▲	▲	▲	▲		▲			▲	▲	▲	
		200hPa	▲						▲				▲	▲	▲
		500hPa											▲	▲	▲
		700hPa													
		850hPa													
		1000hPa													
		Vector Wind	10hPa	▲	▲		▲	▲	▲					▲	▲
	20hPa		▲	▲		▲	▲	▲	▲	▲	▲		▲	▲	▲
	50hPa		▲	▲	▲	▲	▲	▲	▲	▲			▲	▲	▲
	100hPa		▲	▲	▲	▲	▲	▲	▲	▲	▲		▲	▲	▲
	200hPa		▲			▲							▲	▲	
	500hPa		▲			▲							▲	▲	
	700hPa		▲			▲							▲	▲	
	850hPa		▲										▲	▲	
	1000hPa		▲										▲	▲	
	Temp		10hPa	▲	▲		▲			▲				▲	▲
		20hPa	▲	▲		▲	▲	▲	▲	▲			▲	▲	▲
		50hPa	▲	▲		▲	▲	▲	▲	▲	▲		▲	▲	▲
		100hPa	▲	▲	▲	▲	▲		▲				▲	▲	▲
		200hPa	▲			▲							▲	▲	▲
		500hPa													
		700hPa													
		850hPa	▲			▲							▲	▲	
		1000hPa	▲			▲							▲	▲	

345 **Figure 7.** Scorecard of anomaly correlation and RMSE of comparison between AER_cyc and CTL_cyc. Green colors mean AER_cyc is better than CTL_cyc at 95% (filled box), 99% (▲), and 99.9% (▲) significance level. Red colors mean AER_cyc is worse than CTL_cyc at 95% (filled box), 99% (▼), and 99.9% (▼) significance level. Grey boxes mean no statistically significant difference between AER_cyc and CTL_cyc. Blue boxes are not statistically relevant. The statistics are calculated between 20 to 80 degrees of latitude for both hemispheres. The data between 20°S and 20°N is used for the tropical region.

350 **4. Conclusions and Future Outlook**

This article described aerosol absorption and scattering calculations of the CRTM version 2 in the GSI analysis. We also conducted sensitivity experiments to investigate the aerosol-affected GSI analysis in both single-cycle and fully-cycled runs. Both GSI and CRTM are well documented with user guides, tutorials and code repositories available online. This article is

355 primarily a joined-up documentation for aerosol absorption and scattering calculations in the CRTM version 2 and GSI. It also provides guidance for prospective users of the CRTM aerosol option. Scientific aspects of aerosol-affected BT in atmospheric data assimilation are briefly discussed. Specifically, numerical experiments were conducted to illustrate how including aerosol radiative effects in CRTM changes the GSI analysis. We found that taking the aerosols into account reduces simulated BT in thermal window channels over dust-dominant regions. Assimilating aerosol-affected BTs produces a warmer analyzed lower atmosphere. From the verification scorecard, neutral to positive results are found in the fully-cycled, aerosol aware experiment.

360

The CRTM team, in coordination with its partners and collaborators, is building a robust capability to accurately and consistently simulate the emission, absorption, and scattering properties of all (radiatively important) atmospheric constituents. There are several ongoing and planned efforts to enhance the CRTM aerosol module. For example, more aerosol optical look-up tables have been added and the calculations of aerosol optical properties are being evaluated. In addition, the CRTM is being refactored toward a more flexible aerosol interface to handle aerosol optical look-up-tables as well as to support aerosol specifications from other operational aerosol models, such as Community Multiscale Air Quality (CMAQ). Other aerosol-related efforts include, but are not limited to, improving the physical representation of aerosols and including active sensors such as aerosol lidar. These developments, once implemented and tested, will be reported in future manuscripts.

365

Code and Data Availability.

370

Various software packages are referred to throughout the paper. The following list contain links to the main software documentations or repositories discussed:

The GSI webpage: <https://dtcenter.ucar.edu/com-GSI/users/index.php>

The GSI v3.7 user guide: https://dtcenter.ucar.edu/com-GSI/users/docs/users_guide/html_v3.7/index.html

The GSI v3.7 online tutorial: https://dtcenter.ucar.edu/com-GSI/users/tutorial/online_tutorial/index_v3.7.php

375

The DTC community GSI (as of Nov. 29, 2021, via Zenodo): <https://doi.org/10.5281/zenodo.5735601>

The CRTM v2.3.0 public repository (via Zenodo): <https://doi.org/10.5281/zenodo.5695707>

The aerosol related Fortran code in GSI:

Aerosol files check (when `lread_ext_aerosol` is true): `./src/gsi/read_files.f90`

Aerosol data ingestion: `./src/gsi/ncepnmemo_io.f90`, `./src/gsi/general_read_nemsaero.f90`

380

CRTM simulation: `./src/gsi/crtm_interface.f90`

Effective radius setup: `./src/gsi/set_crtm_aerosolmod.f90`

Author Contributions.

QL implemented the aerosol module, CL designed the experiments, and SW performed the experiments. CL prepared the manuscript with contributions from all co-authors.

385 Acknowledgements.

The study of CTL and AER cycled experiments are supported by the Next Generation Global Prediction System (NGGPS) program within NOAA/NWS (award number 352 NA15NWS4680008). The testing and refinement of GSI/CRTM regression test is supported by the DTC Visitor Program. All experiments were conducted at NOAA/NESDIS-funded Supercomputer for
390 Satellite Simulations and Data Assimilation Studies (S4) cluster maintained by Space Science and Engineering Center (SSEC) at University of Wisconsin-Madison. We thank GMAO collaborators, Arlindo da Silva, Mian Chin, and Peter Colarco, for providing valuable input on the calculations of aerosol optical properties for GOCART aerosols.

References

- d'Almeida, G. A., Koepke, P., and Shettle, E.P.: Atmospheric Aerosols: global climatology and radiative characteristics, A. Deepak Publishing, Hampton, VA., 1991.
- 395 American Meteorological Society: Brightness Temperature. Glossary of Meteorology, https://glossary.ametsoc.org/wiki/Brightness_temperature, 2012.
- Binkowski, F. S., Roselle, S. J.: Models-3 Community multiscale air quality (CMAQ) model aerosol component, 1 Model description. *J. Geophys. Res.*, 108, 4183, doi:10.1029/2001JD001409, 2003.
- Buchard, V., da Silva, A. M., Colarco, P. R., Darmonov, A., Randles, C. A., Govindaraju, R., Torres, O., Campbell, J., and
400 Spurr, R.: Using the OMI aerosol index and absorption aerosol optical depth to evaluate the NASA MERRA Aerosol Reanalysis. *Atmos. Chem. Phys.*, 15, 5743–5760, doi:10.5194/acp-15-5743-2015, 2015.
- Bullard, J. E. and Coauthors: High-latitude dust in the Earth system, *Rev. Geophys.*, 54, 447–485, doi:10.1002/2016RG000518, 2016.
- Chen, Y., Weng, F., Han, Y., and Liu, Q.: Planck-Weighted Transmittance and Correction of Solar Reflection for Broadband
405 Infrared Satellite Channels. *J. Atmos. Sci.* 29, 382-396, 2012.
- Chin, M., Ginoux, P., Kinne, S., Torres, O., Holben, B. N., Duncan, B. N., Martin, R. V., Logan, J. A., and Higurashi, A.: Tropospheric aerosol optical thickness from the GOCART model and comparisons with satellite and Sun photometer measurements, *J. Atmos. Sci.*, 59, 461–483, doi:10.1175/1520-0469(2002)059<0461:TAOTFT>2.0.CO;2, 2002.
- Chin, M., Diehl, T., Tan, Q., Prospero, J. M., Kahn, R. A., Remer, L. A., Yu, H., Sayer, A. M., Bian, H., Geogdzhayev, I. V.,
410 Holben, B. N., Howell, S. G., Huebert, B. J., Hsu, N. C., Kim, D., Kucsera, T. L., Levy, R. C., Mishchenko, M. I., Pan, X., Quinn, P. K., Schuster, G. L., Streets, D. G., Strode, S. A., Torres, O., and Zhao, X.-P.: Multi-decadal aerosol variations

- from 1980 to 2009: a perspective from observations and a global model, *Atmos. Chem. Phys.*, 14, 3657–3690, doi.org:10.5194/acp14-3657-2014, 2014.
- 415 Clough, S., Iacano, M. J. and Moncet, J.-L.: Line-by-line Calculations of Atmospheric Fluxes and Cooling Rates: Application to Water Vapor. *J. Geophys. Res.* 97, 15761-15785, 1992.
- Colarco, P., da Silva, A., Chin, M., and Diehl, T.: Online simulations of global aerosol distributions in the NASA GEOS-4 model and comparisons to satellite and ground-based aerosol optical depth, *J. Geophys. Res.*, 115, D14207, doi:10.1029/2009JD012820, 2010.
- 420 Diaz, H. F., Carlson, T. N., and Prospero, J. M.: A study of the structure and dynamics of the Saharan air layer over the northern equatorial Atlantic during BOMEX. National Hurricane and Experimental Meteorology Laboratory NOAA Tech. Memo. ERL WMPO-32, 61 pp, 1976.
- Diaz, J. P., Arbelo, M., Expósito, F.J., Podesta', G., Prospero, J.M., and Evans, R.: Relationship between errors in AVHRR-derived sea surface temperature and the TOMS Aerosol Index, *Geophys. Res. Lett.*, 28, 1989 – 1992, 2001.
- 425 Divakarla, M., and Coauthors: Evaluation of CrIMSS operational products using in-situ measurements, model analysis fields, and retrieval products from heritage algorithms, IEEE International Geoscience and Remote Sensing Symposium, Munich, Germany, 2012, pp. 1046-1049, doi: 10.1109/IGARSS.2012.6350818, 2012.
- Gelaro, R., McCarty, W., Suarez, M. J., Todling, R., and coauthors, 2017: The Modern-Era Retrospective Analysis for Research and Applications, Version 2 (MERRA-2). *J. Climate*, 30, 5419–5454, doi.org: 10.1175/JCLI-D-16-0758.1, 2017.
- 430 Grogan, D., Lu, C.-H., Wei, S.-W., and Chen, S.-P.: Effects of Saharan dust on African easterly waves: The impact of aerosol-affected satellite radiances on data assimilation, *Atmos. Chem. Phys. Disc.*, doi:10.5194/acp-2021-129, 2021.
- Hale, G. M. and Querry, M. R.: Optical constants of water in the 200-nm to 200-mm wavelength region. *Appl. Opt.*, 12, 555–563, 1973.
- Han, Y., van Delst, P., Liu, Q., Weng, F., Yan, B., Treadon, R., and Derber, J.: JCSDA Community Radiative Transfer Model (CRTM) – Version 1, NOAA NESDIS Tech. Rep. 122, 33 pp., NOAA, Silver Spring, Md, 2006.
- 435 Han, Y., Weng, F., Liu, Q., and van Delst, P.: A fast radiative transfer model for SSMIS upper atmosphere sounding channels. *J. Geophys. Res.*, 112, D11121, doi:10.1029/2006JD008208, 2007.
- Hess, M., Koepke, P., Schult I: Optical properties of aerosols and clouds: the software package 1528 OPAC. *Bull Am Met Soc* 79:831–844, 1998.
- 440 Highwood, E. J., Haywood, J. M., Silverstone, M. D., Newman, S. M., and Taylor, J. P.: Radiative properties and direct effect of Saharan dust measured by the C-130 aircraft during Saharan Dust Experiment (SHADE): 2. Terrestrial spectrum, *J. Geophys. Res.*, 108(D18), 8578, doi:10.1029/2002JD002552, 2003.
- Karyampudi, V. M., Palm, S. P., Reagen, J. A., Fang, H., Grant, W. B., Hoff, R. M., Moulin, C., Pierce, H. F., Torres, O., Browell, E. V., and Melfi, S. H.: Validation of the Saharan dust plume conceptual model using lidar, Meteosat, and ECMWF data, *Bull. Am. Meteorol. Soc.*, 80, 1045–1075, doi:10.1175/1520-445 0477(1999)080<1045:VOTSDP>2.0.CO;2.

- Kim, J., Akella, S., da Silva, A.M., Todling, R., McCarty, W.: Preliminary evaluation of influence of aerosols on the simulation of brightness temperature in the NASA's Goddard Earth Observing System Atmospheric Data Assimilation System; Tech. Rep. Ser. Glob. Model. Data Assim., Vol 49, TM-2018-104606, Goddard Space Flight Center, National Aeronautics and Space Administration: Greenbelt, Maryland, US, 2018.
- 450 Kleist, D. T., Parrish, D. F., Derber, J. C., Treadon, R., Wu, W. S., and Lord, S.: Introduction of the GSI into the NCEP Global Data Assimilation System. *Weather and Forecasting*, 24(6):16911705, 2009.
- Letertre-Danczak, J.: The Use of Geostationary Radiance Observations at ECMWF and Aerosol Detection for Hyper-Spectral Infrared Sounders: 1st and 2nd Years Report; EUMETSAT/ECMWF Fellowship Programme Research Reports, Vol 40, European Centre for Medium Range Weather Forecasts: Shinfield Park, Reading, RG2 9AX, England, 2016.
- 455 Liu, Q. and Weng, F.: Advanced doubling-adding method for radiative transfer in planetary atmosphere, *J. Atmos. Sci.*, 63, 3459-3465, doi:10.1175/JAS3808.1, 2006.
- Liu, Q., Han, Y., van Delst, P., and Weng, F.: Modeling aerosol radiance for NCEP data assimilation, in *Fourier Transform Spectroscopy/Hyperspectral Imaging and Sounding of the Environment*, paper HThA5, OSA Technical Digest Series, Optical Society of America, doi:10.1364/HISE.2007.HThA5, 2007.
- 460 Liu, Q. and Lu, C.-H.: Community Radiative Transfer Model for Air Quality Studies. In *Light Scattering Reviews*. 456 Kokhanovsky, A., Eds.; Springer Praxis Books, Springer-Verlag, Berlin – Heidelberg, Germany, Volume 457, pp. 67-115, 2016.
- Liu, Z., Liu, Q., Lin, H.-C., Schwartz, C. S., Lee, Y.-H., and Wang, T.: Three-dimensional variational assimilation of MODIS aerosol optical depth: Implementation and application to a dust storm over East Asia, *J. Geophys. Res.*, 116, D23206, doi:10.1029/2011JD016159, 2011.
- 465 Lu, C.-H., da Silva, A., Wang, J., Moorthi, S., Chin, M., Colarco, P., Tang, Y., Bhattacharjee, P. S., Chen, S.-P., Chuang, H.-Y., Juang, H.-M. H., McQueen, J., and Iredell, M.: The implementation of NEMS GFS Aerosol Component (NGAC) version 1.0 for global dust forecasting at NOAA/NCEP, *Geosci. Model Dev.*, 9, 1905–1919, doi: 10.5194/gmd-9-1905-2016, 2016.
- 470 Matricardi, M.: The inclusion of aerosols and clouds in RTIASI, the ECMWF fast radiative transfer model for the infrared atmospheric sounding interferometer, *ECMWF Tech. Memo.*, 474, doi: 10.21957/1krvb28ql, 2005.
- Merchant, C. J., Embury, O., Le Borgne, P. and Bellec B.: Saharan dust in nighttime thermal imagery: Detection and reduction of related biases in retrieved sea surface temperature, *Remote Sensing of Environ.*, 104, 15–30, doi: 10.1016/j.rse.2006.03.007, 2006.
- 475 Nalli, N. R., and L. L. Stowe, Aerosol correction for remotely sensed sea surface temperatures from the National Oceanic and Atmospheric Administration advanced very high resolution radiometer, *J. Geophys. Res.*, 107(C10), 3172, doi:10.1029/2001JC001162, 2002.

- Pagowski, M., Liu, Z., Grell, G. A., Hu, M., Lin, H.-C., Schwartz, C. S., Implementation of aerosol assimilation in Gridpoint Statistical Interpolation (v3.2) and WRF-Chem (v.3.4.1), *Geosci. Model Dev.*, 7, 1621–1627, doi:10.5194/gmd-7-1621-2014, 2014.
- 480 Petty G: A First Course in Atmospheric Radiation, 2nd edition, Sundog Publishing, Madison, WI, 2006.
- Peyridieu, S., Chdin, A., Tanr, D., Capelle, V., Pierangelo, C., Lamquin, N., and Armante, R.: Saharan dust infrared optical depth and altitude retrieved from AIRS: a focus over North Atlantic comparison to MODIS and CALIPSO, *Atmos. Chem. and Phys. Discuss.*, 9(5):2119921235, 2009.
- 485 Pierangelo, C., Chedin, A., Heilliette, S., Jacquinet-Husson, N., and R. Armante, R.: Dust altitude and infrared optical depth from AIRS. *Atmos. Chem. Phys.*, 4, 1813-1822, doi: 10.5194/acp-4-1813-2004, 2004.
- Randles, C. A., da Silva, A. M., Buchard, V., Colarco, P. R., Darmenov, A., Govindaraju, R., Smirnov, A., Holben, B., Ferrare, R., Hair, J., Shinozuka, Y., Flynn, C., J: The MERRA-2 Aerosol Reanalysis, 1980 Onward. Part I: System Description and Data Assimilation Evaluation, *Journal of Climate*, 30(17), 6823-6850, doi:10.1175/JCLI-D-16-0609.1, 2017.
- 490 Schwartz, C. S., Liu, Z., Lin, H.-C., and Cetola, J. D.: Assimilating aerosol observations with a “hybrid” variational-ensemble data assimilation system, *J. Geophys. Res.-Atmos.*, 119, 4043–4069, doi:10.1002/2013JD020937, 2014.
- Sokolik, I. N.: The spectral radiative signature of wind-blown mineral dust: Implications for remote sensing in the thermal IR region: The spectral radiative signature of wind-blown mineral dust, *Geophys. Res. Lett.*, 29, 7-1-7-4, doi:10.1029/2002GL015910, 2002.
- 495 Stegmann, P. G., Tang, G., Yang, P. and Johnson, B. T.: A stochastic model for density-dependent microwave Snow- and Graupel scattering coefficients of the NOAA JCSDA community radiative transfer model, *J. Quant. Spec. Rad. Trans.*, 211, 9-24, doi:10.1016/j.jqsrt.2018.02.026, 2018.
- Ukhov, A., Ahmadov, R., Grell, G., and Stenchikov, G.: Improving dust simulations in WRF-Chem model v4.1.3 coupled with GOCART aerosol module, *Geosci. Model Dev. Disc.*, doi:10.5194/gmd-2020-92, 2021.
- 500 Wang, J., Bhattacharjee, P.S., Tallapragada, V., Lu, C.-H., Kondragunta, S., da Silva, A., Zhang, X., Chen, S.-P., Wei, S.-W., Darmenov, A.S., et al.: The implementation of NEMS GFS Aerosol Component (NGAC) Version 2.0 for global multispecies forecasting at NOAA/NCEP – Part 1: Model descriptions., *Geosci. Model Dev.*, 11, 2315–2332, doi:10.5194/gmd-11-2315-2018, 2018.
- Weaver, C. J., Joiner, J., and Ginoux, P.: Mineral aerosol contamination of TIROS Operational Vertical Sounder (TOVS) temperature and moisture retrievals., *J. Geophys. Res.*, 108, doi:10.1029/2002JD002571, 2003.
- 505 Wei, S.-W., Lu, C.-H., Liu, Q., Collard, A., Zhu, T., Grogan, D., Li, X., Wang, J., Grimblin, R., and Bhattacharjee, P.: The impact of aerosols on satellite radiance data assimilation using NCEP global data assimilation system, *Atmos.*, 12(4), 432, doi:10.3390/atmos12040432, 2021a.
- Wei, S.-W., Lu, C.-H., Johnson, B. T., Dang, C., Stegmann, P., Grogan, D., Ge, G., and Hu, M.: The influence of aerosols on satellite infrared radiance simulations and Jacobians: Numerical experiments of CRTM and GSI, *Remote. Sens.*, in review, 2021b.
- 510

Weng, F.: Advances in radiative transfer modeling in support of satellite data assimilation. *J. Atmos. Sci.*, 64, 3799–3807, doi:10.1175/2007JAS2112.1, 2007.

515 Wu, W.-S., Purser, R. J., and Parrish, D. F.: Three-dimensional variational analysis with spatially inhomogeneous covariances, *Mon. Weather Rev.*, 130, 2905–2916, doi:10.1175/1520-0493(2002)130<2905:TDVAWS>E2.0.CO;2, 2002.

Wu, M., Liu, X., Yu, H., Wang, H., Shi, Y., Yang, K., Darmenov, A., Wu, C., Wang, Z., Luo, T., Feng, Y., and Ke, Z.: Understanding processes that control dust spatial distributions with global climate models and satellite observations, *Atmos. Chem. Phys.*, 20, 13835–13855, <https://doi.org/10.5194/acp-20-13835-2020>, 2020.

520 Zhang L., Grell, G.A., Montuoro, R., McKeen, S. A., Bhattacharjee, P. S., Baker, B., Henderson, J., Pan, L., Frost, G. J., McQueen, J., Saylor, R., Ahmadov, R., Li, H., Wang, J., Stajner, I., Kondragunta, S., Zhang, X., Li, F.: Development of GEFS-Aerosols into NOAAs Unified Forecast System UFS., *Geosci. Model Dev. Discuss.*, doi:10.5194/gmd-2021-378, 2021.